CFD Analysis of Shell and Tube Heat Exchanger to Study the Effect of Baffle Cut on the Pressure Drop and Heat Transfer Coefficient

Chetan Namdeo Patil[1] N. S. Bhalkikar[2]
[1]PG student [2]Professor
[1,2]Department of Mechanical Engineering
[1,2]MIT Aurangabad, India

Abstract— The shell side design of a shell-and-tube heat exchanger; in particular the baffle spacing, baffle cut and shell diameter dependencies of the heat transfer coefficient and the pressure drop are investigated by numerically modeling a small heat exchanger. The flow and temperature fields inside the shell are resolved using a commercial CFD package. A set of CFD simulations is performed for a single shell and single tube pass heat exchanger with a variable number of baffles and turbulent flow. The results are observed to be sensitive to the turbulence model selection. The best turbulence model among the ones considered is determined by comparing the CFD results of heat transfer coefficient, outlet temperature and pressure drop with the Bell–Delaware method results. For two baffle cut values, the effect of the baffle spacing to shell diameter ratio on the heat exchanger performance is investigated by varying flow rate.
Key words: CFD, Heat exchangers, Shell-and-tube, Baffle spacing, Turbulence models.

I. INTRODUCTION

Shell and tube heat exchangers are known as the work-horse of the chemical process industry when it comes to transferring heat. These devices are available in a wide range of configurations as defined by the Tubular Exchanger Manufacturers Association. The applications of single-phase shell-and-tube heat exchangers are quite large because these are widely in chemical, petroleum, power generation and process industries. In essence, a shell and tube exchanger is a pressure vessel with many tubes inside of it. One process fluids flows through the tubes of the exchanger while the other flows outside of the tubes within the shell. The tube side and shell side fluids are separated by a tube sheet. In these heat exchangers, one fluid flows through tubes while the other fluid flows in the shell across the tube bundle. The design of a heat exchanger requires a balanced approach between the thermal design and pressure drop. The performance parameters include heat transfer, pressure drop, effectiveness etc. The determination of pressure drop along with heat transfer in a heat exchanger is essential for many applications for at least two reasons:

(1) The fluid needs to be pumped through the exchanger, which means that fluid pumping power is required. This pumping power is proportional to the exchanger pressure drop.

(2) The heat transfer rate can be influenced significantly by the saturation temperature change for a condensing/evaporating fluid in case of multiphase flow if there is a large pressure drop associated with the flow. Ideally most of the pressure drop available should be utilized in the core and a small fraction in the manifolds, headers, or other flow distribution devices.

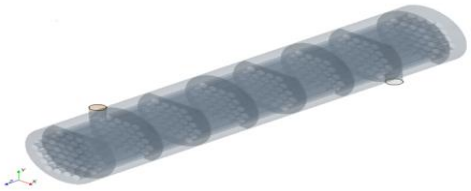

Fig. 1: The model with 8 baffles

To be able to understand the causes of the shell side design weaknesses, the flow phenomenon inside the shell must be well understood. For that purpose, numerous analytical, experimental and numerical studies have been performed. Most of these studies were concentrated on the certain aspects of the shell-and-tube heat exchanger design. Among others, Gay et al. [4] worked on heat transfer, while Halle et al. [5], Pekdemir et al. [6], Gaddis and Gnielinski [7] investigated pressure drop. Some of the researchers concentrated only on certain parts of the shell-and-tube heat exchanger. It can be particularly useful in the initial design steps, reducing the number of testing of prototypes and providing a good insight in the transport phenomena occurring in the heat exchangers [14]. In all of these simplified approaches, the shell side pressure drop and heat transfer rate results showed good agreement with experimental data.

II. EXPERIMENTATION

The experimental set up consists of 1 in 2 pass shell and tube heat exchanger as shown. The hot and cold water tanks are of 200 litres capacity. The hot water tank is provided with heaters of 8 KWh capacity. The hot and the cold water is pumped by centrifugal pump. The flow rates are measured by pre calibrated rotameters. The rotameter range is 60 kg/hr upto 600 kg/hr. Thermocouples are provided at inlets and outlets of the heat exchanger to know the temperatures of the shell side and tube passes. Bypass valves at both sides are provided to vary flow rates. The temperature scanner is provided with temperature display along with channel number. The provision for automatic/manual advance for temperature measurement is made in the temperature scanner. Also start switches for heaters and water pumps are provided in the temperature scanner. The temperature scanner is connected to the power supply.

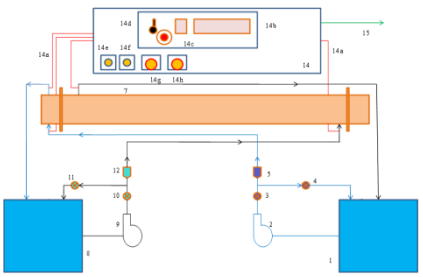

Fig. 2: Experimental set up of Shell and Tube Heat Exchanger

1. Cold water tank 2. Cold water pump 3. Cold water flow adjusting/controlling valve 4. Cold water bypass valve 5. Rotameter 7.Shell and Tube heat exchanger 8. Hot water tank 9.Hot water pump 10. Hot water flow adjusting/controlling valve 11. Hot water bypass valve 12. Rotameter 14.Temperature scanner a)Cables from thermocouples to panel b) Temperature display with channel number c) Manual advance of channel d) Automatic/Manual advance switch e) Hot water pump start switch f) Cold water pump start switch g) Heater A start switch h) Heater B start switch 15. To power supply

Sr.No.	**Shell side fluid**			**Tube side fluid**		
	Mass flow rate	Shell inlet temp.	Shell oulet temp.	Mass flow rate	Tube inlet temp.	Tube outlet temp.
	kg/hr	^{0}C	^{0}C	kg/hr	^{0}C	^{0}C
1	60	60	34.3	300	33.8	33.9
2	120	59.3	35.6	300	33.8	34.5
3	180	59	37.2	300	33.7	35.5
4	240	58.1	39.1	300	33.7	37.3
5	300	57.4	40.2	300	33.7	38.4
6	360	56.8	41.8	300	33.7	41.1
7	420	54.8	44.2	300	35.1	44.6
8	480	54.4	44.6	300	35.4	44.9
9	540	53.1	44.9	300	35.8	45.2
10	600	53.5	45.8	300	36.2	45.6

Table 1: Temperature measurements

The table depicts the variation of temperatures with the change in mass flow rate. The tube side temperature difference increases with the increase in mass flow rates.

III. PRESSURE MODEL

A. Pressure drop in the inlet and outlet nozzles (Δpn): For computing the pressure drops in both inlet and outlet nozzles in an heat exchanger, the expression used is given by Eq. (1.1). This pressure drop for both the nozzles together is designated by Δp_n

$$\Delta p_n = \frac{\rho_s \varepsilon_n u_n^2}{2} \quad \ldots\ldots (1.1)$$

As ε_n has been taken as 2.0 and eqn.1 becomes as

$$\Delta p_n = \rho_s u_n^2 \quad \ldots\ldots (1.2)$$

A. Pressure drop in the interior compartments cross flow section (Δp_c):

The modeling for pressure loss under this section has been presented in two parts as given below:

(1) Pressure drop across the tube bundle.

(2) Pressure drop in the window section.

B. Modeling for pressure drop across the tube bundle:

To model pressure drop across the tube bundle, the beginning has been made using the pressure drop expression for the flow across tube bundle which is reproduced here by Eq. (2.1).

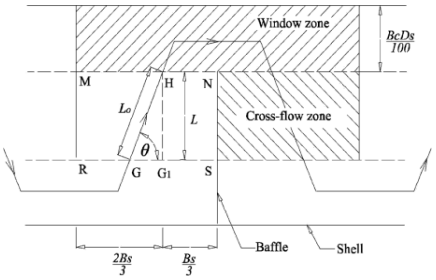

Fig. 3: Delination of cross-flow and window zones

$$\Delta p_c = \frac{\rho_s f L u_{sc}^2}{2P_p} \quad \ldots\ldots (2.1)$$

In Eq. (2.1) given above, L has been determined assuming the vertical flow i.e. in G_1H direction as illustrated in Fig. 2. However, the actual flow direction is shown by GH line, which is inclined from horizontal by an angle θ. In the present work instead of flow direction G_1H has been approximated by GH (Fig. 2). The angle θ has been illustrated in the same diagram. In view of the above, L in Eq. (2.1) has been replaced by GH, which has been taken equal to L_0. Substituting L_0 in place of L in Eq. (2.1), we get Eq. (2.2).

$$\Delta p_c = \frac{\rho_s f L_0 u_{sc}^2}{2P_p} \quad \ldots\ldots (2.2)$$

Referring to Fig.2, we get $L_0 = L/\sin\theta$ and now making this substitution, Eq. (2.2) becomes Eq. (2.3).

$$\Delta p_c = \frac{\rho_s f u_{sc}^2}{2P_p} \frac{L}{\sin\theta} \quad \ldots\ldots (2.3)$$

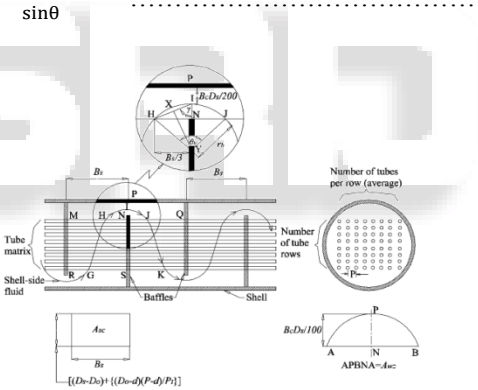

Fig. 4: Showing the actual flow pattern in shell-side

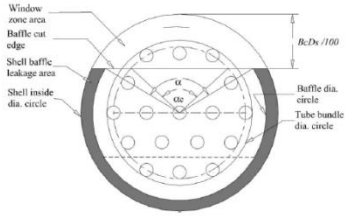

Fig. 5: Illustration of baffle cut angles, leakage area

C. Pressure drop in window section zone (Δp_{wz}):

The pressure drop in convergent–divergent nozzle is given by Eq. (3.1).

Δp_{cdn} = 2* Pressure drop in convergent nozzle …….. (3.1)

Δp_{cdn} is given by Eq. (3.2). In the window section zone, there is no effect of bundle bypass leakage and therefore ignored here.

$$\Delta p_{cdn} = \frac{2\rho_s u_{sc}^2}{2} [(A_{sc} / A_{wz})^2 - 1](\mu_{sw} / \mu_s)^{0.14} \quad \ldots\ldots (3.2)$$

A_{wz} = window area excluding the area of tubes in window zone

Referring to Fig. 4 window area including tubes,

$$\Delta p_c = \left\{\frac{\pi D_S^2}{4}\frac{\alpha}{360} - \left[\frac{D_S^2}{4}\left(1-\frac{2B_c}{100}\right)D_b \sin\left(\frac{\alpha}{2}\right)\right] - N_{wt}\frac{\pi d^2}{4}\right\} \quad (3.3)$$

where, Area of window tubes = $N_{wt}\frac{\pi d^2}{4}$

D. Determination of pressure drop due to flow stream bend (Δp_b) in the window section:

The procedure given in reference [10] has been followed to compute the pressure loss in a bend. According to this procedure Δp_b is expressed by Eqs. (4.1).

$$\Delta p_b = \frac{\rho_s k u_{wz}^2}{2} \quad \ldots\ldots (4.1)$$

$$\text{where, } u_{wz} = \frac{\dot{V}}{A_{wz}} \quad \ldots\ldots (4.2)$$

$$\Delta pwz' = \Delta p_b + \Delta p_{cdn} \quad \ldots\ldots (4.3)$$

The final equation of Δpwz is given by Eqs. (4.4).

$$\Delta p_{wz} = \Delta pwz' * \frac{B_s}{D_s} \quad \ldots\ldots (4.4)$$

The total pressure drop in the interior compartments is given by Eq. (10b).

$$\Delta p_{ic} = (N_b - 1)\,\Delta p_c + N_b \Delta p_{wz} \quad \ldots\ldots (4.5)$$

E. Pressure drop in end cross-sections due to fluid flow across the tube bundle:

On the basis of discussion given here to compute the pressure loss at inlet and outlet sections the expression given in Ref. [12] has been used in the present work, which is given here by Eq. (5.1).

$$\Delta p'_{ec} = \frac{\rho_s f u_{sc}^2}{2} N_c \left(1+\frac{N_w}{N_c}\right) f_b f_s (\mu sw / \mu s)^2 \quad \ldots\ldots (5.1)$$

Here f_b and f_s equal to 1 or here neglecting them because there is no leakage and presence of equal baffle spacing. The values of N_w, N_c have been computed using the expressions given by Taborek [8]. For both the end sections, the total pressure drop Δp_{ec} is obtained after multiplying $\Delta p'_{ec}$ by 2 and finally is given by Eq. (5.2).

$$\Delta p_{ec} = 2\,\Delta p'_{ec} \quad \ldots\ldots (5.2)$$

F. Total pressure drop in the shell:

The total pressure drop is given by Eq. (5.3).

$$\Delta p_s = \Delta p_n + (N_b - 1)\Delta p_c + N_b\,\Delta p_{wz} + \Delta p_{ec} \quad \ldots\ldots (5.3)$$

IV. Simulation Results

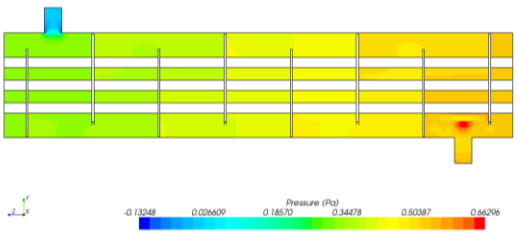

Fig. 6: Scalar contour of pressure across section plane for 60 kg/hr

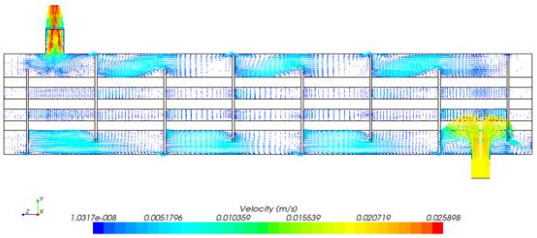

Fig. 7: Velocity vectors across section plane for 60 kg/hr

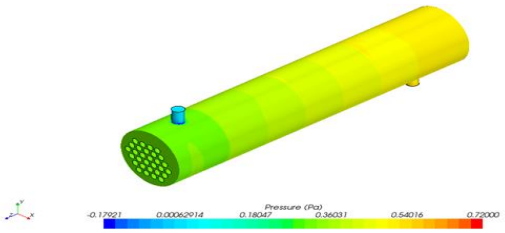

Fig. 8: Scalar contour of pressure for 60 kg/hr

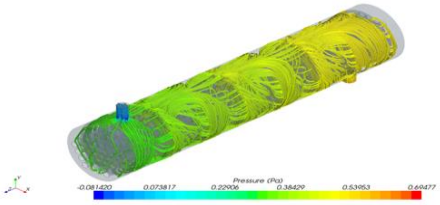

Fig. 9: Streamlines showing pressure variation for 60 kg/hr

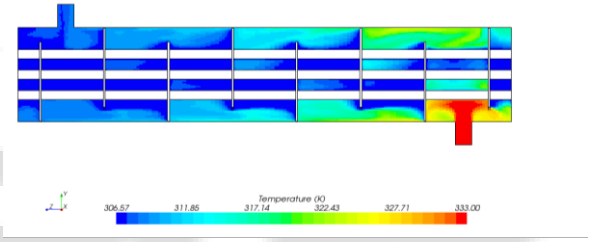

Fig. 10: Scalar contour of temperature across section plane for 60 kg/hr

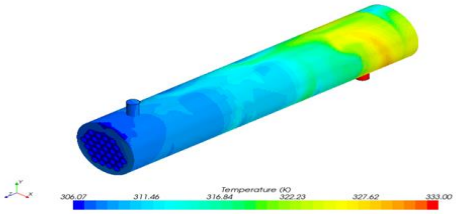

Fig. 11: Scalar contour of temperature for 60 kg/hr

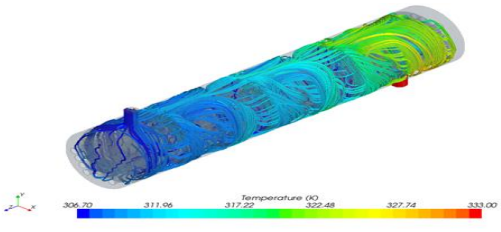

Fig. 12: Streamlines showing temperature variation for 60 kg/hr

V. Validation

A. Shell side pressure drop results validation:

The comparison of present model results has been done with experimental results. The total Reynolds numbers range

covered lies between 10^3 and 10^5. It would be worth to mention that the present model results compare well with experimental results for the fluids, water and oil flowing on the shell-side. This shows that the results of the present model match more closely with the experimental results [2]. Hence the pressure model is validated with the experimental results for the above range of Reynolds number.

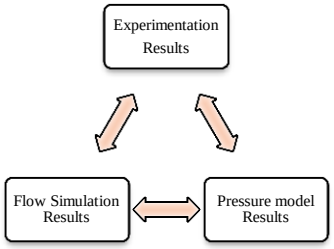

Fig. 13: Validation

As the pressure model is validated for Reynolds number 10^3 to 10^5 so it used for the validation of simulation results for the above range of Reynolds number.

Percentage error for shell side pressure drop:

The percentage error is given by,
Error (%) = [(Pressure model value – Simulation value) / Pressure model value] X100

Sr. No.	Mass flow rate	Pressure model Results	Simulation results	Percentage Error
	kg/sec	Pa	Pa	%
1	0.01666	0.47735686	0.559493	-17.20644
2	0.03333	1.89152035	1.98434	-4.907145
3	0.05	4.23486431	4.303975	-1.631945
4	0.06666	7.49861295	7.500554	-0.025885
5	0.08333	11.6851262	11.508868	1.508398
6	0.1	16.7927480	16.518	1.636111
7	0.11666	22.8007505	22.0399	3.336953
8	0.13333	29.7307042	28.646683	3.646133
9	0.15	37.5724503	36.135445	3.824624
10	0.16666	46.3468743	44.467651	4.054692

Table 2: Calculation of Percentage Error

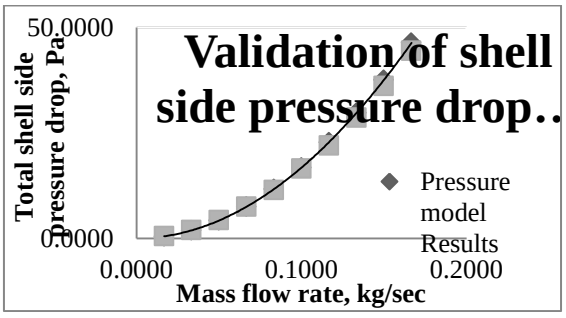

Fig. 14: Validation of pressure model results and simulation results

B. Relation between results:

The graph between the pressure model value for shell side pressure drop and the simulation value for the shell side pressure drop follow linear relationship in the range of mass flow rates between 60 kg/hr to 600 kg/hr.

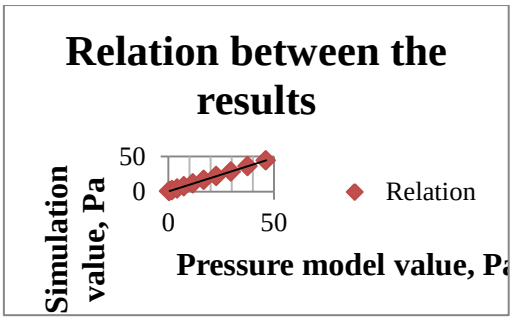

Fig. 15: Relationship trend of the results

C. Shell side heat transfer co-efficient:

Sr.No.	Re_s	k of water	Experimental results		Simulation Results		Co-Relation results	
			h_{shell}	Nu_s	h_{shell}	Nu_s	h_{shell}	Nu_s
		W/mK	W/m^2K		W/m^2K		W/m^2K	
1	1029.22	0.624	217.9157455	58.43634218	77.5518224	20.79631658	302.2045409	77.4402607
2	2028.65	0.624	359.7576023	96.47269086	148.9886671	39.95283916	441.102152	113.0329331
3	3043.29	0.624	471.7760681	126.5115914	221.5778094	59.41836219	551.3320714	141.2794765
4	3998.26	0.624	543.4850792	145.7410982	291.698355	78.22190567	641.7900779	165.2184882
5	4916.54	0.628	689.5391423	183.7292416	365.407471	97.36363525	723.0432644	186.1358085
6	5899.87	0.628	808.8703137	215.5252983	415.3355165	110.6670743	799.3094095	205.7692956
7	6677.94	0.631	774.1511118	205.2935877	502.7167474	133.3131518	862.1111411	222.7934849
8	7512.92	0.631	996.7858882	264.3330844	612.7576507	162.4943949	924.665451	238.9592575
9	8306.24	0.631	1146.507994	304.037204	757.556798	200.8930176	982.3384581	254.059751
10	9391.01	0.631	1210.598482	321.0330668	929.9331374	246.6047096	1044.859495	270.2294112

Fig. 16: Nusselt Number for 25% baffle cut

VI. BAFFLE CUT ANALYSIS

The validation of the simulation enables to carry out further the change in baffle parameters. The variation of the baffle parameters and getting results through simulation is a key for optimizing baffle parameters. Hence the baffle cut is preferred for variation as the effect of baffle cut is more pronounced than baffle spacing. The baffle cut is in the range of 20% - 35% as specified for this type of heat exchanger. Hence baffle cut is to be varied in this range only.

Sr.No.	Simulation Results for 30% baffle cut	
	M	ΔP_s
	kg/sec	Pa
1	0.01666	0.539655
2	0.03333	1.903972
3	0.05	4.11122
4	0.06666	7.165568
5	0.083333	11.008043
6	0.1	15.611549
7	0.11666	21.101822
8	0.13333	27.444256
9	0.15	34.566093
10	0.16666	42.515915

Fig. 17: Simulation results for shell side pressure drop with 30% baffle cut

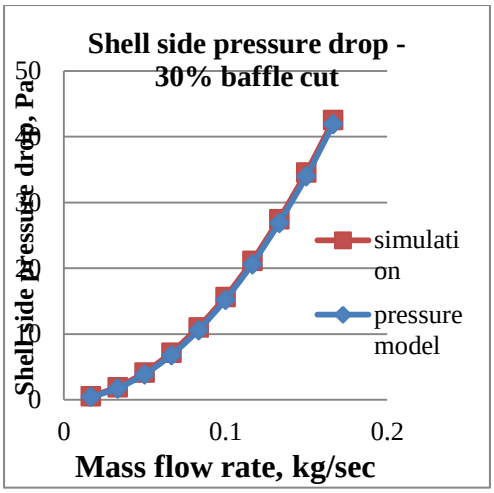

Fig. 18: Shell side pressure drop as a function of mass flow rate for 30% baffle cut

VII. COMPARISON OF RESULTS

A. *Shell side pressure drop:*

Sr.No.	Mass flow rate	25% ΔP_s	30% ΔP_s	% Decrease
1	kg/sec	Pa	Pa	
2	0.01666	0.559493	0.539655	3.545710134
3	0.03333	1.98434	1.903972	4.05011238
4	0.05	4.303975	4.11122	4.478534378
5	0.06666	7.500554	7.165568	4.4661501
6	0.08333	11.508868	11.008043	4.351644315
7	0.1	16.518	15.611549	5.487655891
8	0.11666	22.0399	21.101822	4.25627158
9	0.13333	28.646683	27.444256	4.197438845
10	0.15	36.135445	34.566093	4.342971285
11	0.16666	44.467651	42.515915	4.389114235

Fig. 19: Shell side pressure drop value for baffle cuts

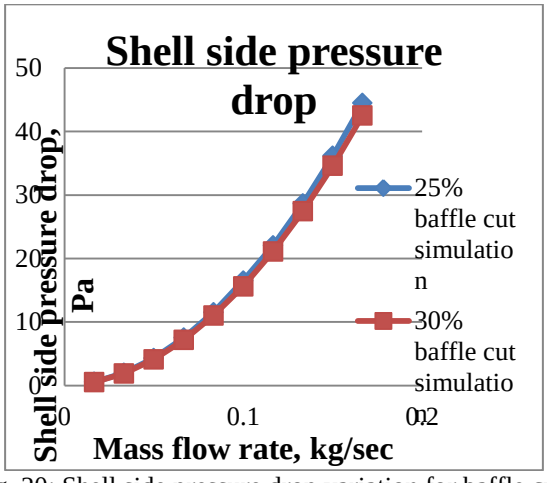

Fig. 20: Shell side pressure drop variation for baffle cuts

B. *Shell side heat transfer co-efficient:*

Sr.No.	Mass flow rate	25% h_{shell}	30% h_{shell}	% Decrease
	kg/sec	W/m^2K	W/m^2K	
1	0.01666	77.5518224	75.95687725	2.056618531
2	0.03333	148.9886671	147.8426053	0.769227467
3	0.05	221.5778094	211.2609566	4.656085773
4	0.06666	291.698355	271.9678896	6.763996101
5	0.08333	365.407471	345.9926972	5.313184698
6	0.1	415.3355165	414.6823839	0.157254229
7	0.11666	502.7167474	494.5568196	1.623166094
8	0.13333	612.7576507	601.747373	1.796840498
9	0.15	757.556798	748.1716606	1.23886914
10	0.16666	929.9331374	917.6621827	1.319552362

Fig. 21: Shell side heat transfer coefficients values for baffle cuts

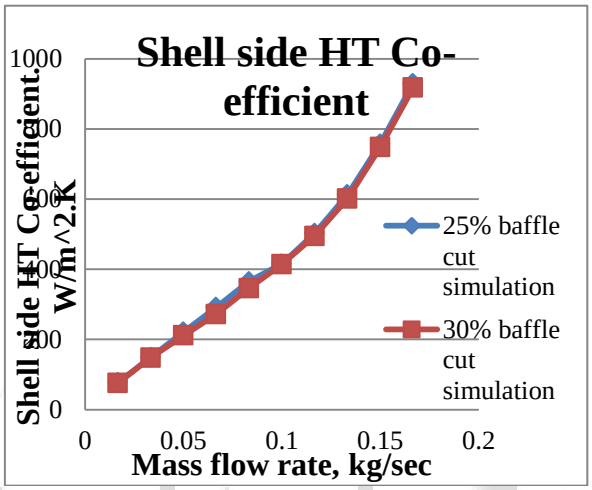

Fig. 22: Shell side heat transfer co-efficient variation for baffle cuts

VIII. CONCLUSION

The effect of baffle cut and baffle spacing on the shell side pressure drop and the shell side heat transfer co-efficient has been studied using the pressure model and simulation. It is therefore concluded that

(1) The shell side fluid flow will be governed by the baffle geometry.
(2) The pressure model gives a complete picture of shell side pressure drop distribution in the interior zone.
(3) The use of pressure model is costless rather than manufacturing the shell and tube heat exchanger for different baffle cut and spacing. The use of model is economical.
(4) The CFD software FLUENT 4.04.011 is valid for determining the shell side pressure drop of the shell and tube heat exchanger taken for analysis under the assumed condition within permissible errors.
(5) The validation of the shell side pressure drop simulations results presents a better substitute for comparing the results with the pressure model.
(6) The simulation visualizes the complete interior phenomena of shell side pressure drop across baffles and the tube bundle.

(7) The shell side pressure drop is less for 30% baffle cut.
(8) The shell side heat transfer coefficient is also affected by the baffle geometry.
(9) The shell side heat transfer coefficient for 30% baffle cut is almost same as that for 25% baffle cut.
(10) The shell side pressure drop is less for 30% baffle cut. The shell side heat transfer co-efficient is almost the same as that for 25% baffle cut, for higher flow rates. Hence 30% baffle cut should be preferred for higher flow rates.
(11) The simulation is better option in the optimization of baffle geometry for effective shell side pressure drop utilization along with the shell side heat transfer co-efficient. As it incorporates the advantages of both experimentation as well as pressure model analysis.
(12) It is rather beneficial to simulate than refabricate the existing shell and tube heat exchanger setup as economy, time is considered.

REFERENCES

[1] Gaddis D, editor. Standards of the Tubular Exchanger Manufacturers Association. Tarrytown (NY): TEMA Inc.; 2007.
[2] Kern DQ. Process heat transfer. New York (NY): McGraw-Hill; 1950.
[3] Bell KJ. Delaware method for shell side design. In: Kakaç S, Bergles AE, Mayinger F, editors. Heat exchangers: thermal–hydraulic fundamentals and design. New York: Hemisphere; 1981. p. 581–618.
[4] Gay B, Mackley NV, Jenkins JD. Shell-side heat transfer in baffled cylindrical shell-and-tube exchangers – an electrochemical mass transfer modeling technique. Int J Heat Mass Transfer 1976;19:995–1002.
[5] Halle H, Chenoweth JM, Wabsganss MW. Shell side water flow pressure drop distribution measurements in an industrial-sized test heat exchanger. J Heat Transfer 1988;110:60–7.
[6] Pekdemir T, Davies TW, Haseler LE, Diaper AD. Pressure drop measurements on the shell side of a cylindrical shell-and-tube heat exchanger. Heat Transfer Eng 1994;15:42–56.
[7] Gaddis ES, Gnielinski V. Pressure drop on the shell side of shell-and-tube heat exchangers with segmental baffles. Chem Eng Process 1997;36:149–59.
[8] Li HD, Kottke V. Visualization and determination of local heat transfer coefficients in shell-and-tube heat exchangers for staggered tube arrangement by mass transfer measurements. Exp Therm Fluid Sci 1998;17:210–6.
[9] Li HD, Kottke V. Visualization and determination of local heat transfer coefficients in shell-and-tube heat exchangers for in-line tube arrangement by mass transfer measurements. Heat Mass Transfer 1998;33:371–6.
[10] Karno A, Ajib S. Effect of tube pitch on heat transfer in shell-and-tube heat exchangers – new simulation software. Heat Mass Transfer 2006;42:263–70.
[11] Sparrow EM, Reifschneider LG. Effect of interbaffle spacing on heat transfer and pressure drop in a shell-and-tube heat exchanger. Int J Heat Mass Transfer 1986;29:1617–28.
[12] Eryener D. Thermoeconomic optimization of baffle spacing for shell and tube heat exchangers. Energy Convers Manage 2006;47:1478–89.
[13] Karno A, Ajib S. Effects of baffle cut and number of baffles on pressure drop and heat transfer in shell-and-tube heat exchangers – numerical simulation. Int J Heat Exchangers 2006;7:299–322.
[14] Sunden B. Computational heat transfer in heat exchangers. Heat Transfer Eng 2007;28:895–7.
[15] Incropera FP, Dewitt DP. Fundamentals of heat and mass transfer. 4th ed. New York: John Wiley; 1996.
[16] Kapale U C, Chand S. Modeling for shell-side pressure drop for liquid flow in shell-and-tube heat exchanger. Int J Heat Mass Transfer 2006;49:601–10.
[17] Taborek J. Thermal and hydraulic design of heat exchangers. In: Hewitt GF, editor. Heat exchangers design handbook, vol. 3. New York: Begell House Inc.; 2002.
[18] Mukherjee R. Effectively design shell-and-tube heat exchangers. Chem Eng Prog 1998;94:21–37.

